

Magnetic amplitude inversion for depth-to-basement and apparent magnetization-intensity estimates

Marlon C. Hidalgo-Gato¹, Valéria C. F. Barbosa², and Vanderlei C. Oliveira Jr.²

ABSTRACT

We have developed an inversion method to recover the depth and the total magnetization intensity of the basement under a sedimentary basin using the amplitude of the magnetic anomaly vector (amplitude data). Because the amplitude data are weakly dependent on the magnetization direction, our method is suitable for interpreting areas with remanent magnetization. Our method assumes constant magnetized basement rocks overlain by nonmagnetic sediments. To overcome the inherent ambiguity of potential field data, we assume knowledge of the average depth of the basement and use it as a constraint to regularize the inversion. A sensitivity analysis with synthetic data shows the weak dependency of the magnetic amplitude inversion on the magnetization direction. Different combinations of magnetization directions recover the interface separating sediments from basement rocks. Test on field data over the Foz do Amazonas Basin, Brazil, recovers the shape of the basement relief without any knowledge about the magnetization intensity and direction. The estimated basement relief reveals a smooth basement framework with basement highs in the central part of the area. In a regional-scale perspective, the deeper and constant estimated basement relief at the northernmost limit of the area may suggest changing in crustal domains from a hyperextended continental crust to homogeneous oceanic crust.

INTRODUCTION

The most widely used magnetic data for estimating the depth to sources are the total-field anomaly. Total-field anomaly inversion requires knowledge about the total magnetization vector of the

sources. Usually, geophysicists assume a purely induced magnetization. If this assumption is not satisfied, erroneous depth-to-basement estimates are obtained from total-field anomaly inversion; hence, the remanent magnetization cannot be neglected.

Conversely, the amplitude of the magnetic anomaly vector is weakly dependent on the magnetization direction (Shearer and Li, 2004; Li et al., 2010). The amplitude of the magnetic anomaly vector is defined as the square root of the sum of the squares of the x -, y - and z -components of the magnetic anomaly vector. These components can be measured (Christensen and Dransfield, 2002; Dransfield et al., 2003), but they are rarely surveyed. Usually, they are calculated from the total-field anomaly either in the wave-number domain (Lourenco and Morrison, 1973; Pedersen, 1978) or in the space domain through the equivalent-layer technique (Dampney, 1969).

In the case of 2D magnetic bodies, the amplitude of the magnetic anomaly vector is the envelope of the x - and z -components of the magnetic anomaly vector (Nabighian, 1972), regardless of the source magnetization direction. However, in geologic scenarios with 3D magnetic bodies, the amplitude of the magnetic anomaly vector depends on the source magnetization weakly (Nabighian, 1984; Haney et al., 2003). The weak dependence on the source magnetization direction makes the amplitude of the magnetic anomaly vector an efficient data for interpreting geologic settings with remanently magnetized sources.

The magnetic data in basin-scale studies have been used to delineate structural features within the basement (e.g., structural highs and lows, terraces, ridges, and faults) yielding a structural map (Carvalho et al., 2012; Lourenco et al., 2014; Hidalgo-Gato and Barbosa, 2015; Ali et al., 2017). The tectonic processes sculpt the basement structures, which, in turn, control the basin architecture. Hence, the structural framework of the basement in depth is important to understand the basin evolution and to assist in hydrocarbon exploration efforts. Spectral analysis of the magnetic data has been widely used to estimate the average depths of ensembles

Manuscript received by the Editor 4 November 2019; revised manuscript received 9 September 2020; published ahead of production 8 October 2020; published online 5 January 2021.

¹Observatório Nacional, Gal. José Cristino, 77, São Cristóvão, Rio de Janeiro 20921-400, Brazil and Shell, Down Town, Rio de Janeiro, Brazil. E-mail: marlonchg@hotmail.com (corresponding author).

²Observatório Nacional, Gal. José Cristino, 77, São Cristóvão, Rio de Janeiro 20921-400, Brazil. E-mail: valcris@on.br; vanderlei@on.br.
© 2021 Society of Exploration Geophysicists. All rights reserved.

of shallow- and deep-seated magnetic sources (Spector and Grant 1970) where the shallow-seated magnetic sources can be intrasedimentary mafic and ultramafic bodies and the deep-seated magnetic sources can be the basement. To estimate the basement relief, some methods estimate the depth to the basement at discrete points by using Parker's (1973) forward method, which computes the magnetic field produced by an interface in the Fourier domain. Because of that, we call such methods "spectral inversions" (Oldenburg, 1974; Guspi, 1993; Caratori Tontini et al., 2008). Using a nonspectral approach, some methods (Zeyen and Pous, 1991; Mickus and Peeples, 1992; Gallardo-Delgado et al., 2003; Nunes et al., 2008; Hidalgo-Gato and Barbosa, 2019) parameterize the basement into a grid of prisms (2D or 3D) to estimate the shape of the basement topography subject to fit the observed total-field anomaly in the space domain.

Here, we follow a nonspectral approach to parameterize the basement through a grid of juxtaposed rectangular prisms. Differently from the previous nonspectral inversions, we invert the amplitude of the magnetic anomaly vector for simultaneously estimating the depths of the basement relief and the apparent magnetization intensity of the basement rocks. We assume the absence of intrasedimentary igneous intrusions and prior knowledge about the average basement depth. The method requires a uniform magnetization for the basement rocks; however, it does not assume a given magnetization vector. We do not compute the three orthogonal components of the magnetic anomaly produced by prisms through 3D integrals (Bhattacharyya, 1964). Rather, we use the fast-forward modeling based on the Gauss-Legendre quadrature (GLQ) proposed by Hidalgo-Gato and Barbosa (2019). Tests on synthetic data and on field data collected over the Foz do Amazonas Basin, Brazil, confirm the potential of our method in retrieving the shape of the basement without specifying the magnetization direction and intensity of the sources.

METHODOLOGY

Forward model

We assume a sedimentary basin with no magnetic sediments or intrusions. We assume that its crystalline basement has a constant but unknown magnetization vector with inclination m_i , declination m_d , and intensity m . Consider a Cartesian coordinate system with the x - and y -axes oriented, respectively, to the north and east and the vertical axis (z -axis) positive downward. We parameterize the magnetic basement with a collection of M prisms with tops at the interface between sediments and basement and bottoms at an arbitrary constant depth Z_b tending to infinite. The depths of the tops of the prisms p_j , $j = 1, \dots, M$, define the basement relief and together with the magnetization intensity (m) are the parameters to be estimated from the magnetic anomaly vector amplitude.

To calculate the forward modeling of the α -component, $\alpha = x, y, z$, of the magnetic anomaly vector produced by a prism, we adopted the same methodology presented by Hidalgo-Gato and Barbosa (2019) to compute the total-field anomaly of a prism, which is named the fast-prismatic forward modeling. Like Hidalgo-Gato and Barbosa (2019), we approximate the 3D integral (volume integral) of the α -component of the magnetic anomaly vector produced by the j th prism, at the observation point (x_i, y_i, z_i) with unity magnetization intensity and horizontal cross section, by a 1D integral along the prism thickness considering the limits of

the integration as the depths to the top p_j (depth to the basement) at the j th prism and the depth to the base Z_b

$$b_{ij}^\alpha \approx C_m \Delta s \frac{\partial}{\partial \alpha} \int_{p_j}^{Z_b} \hat{\mathbf{h}} \bullet \nabla \frac{1}{r_{ij}} dz', \quad (1)$$

where $C_m = \mu_0/4\pi = 10^{-7}$ (in Henry·m⁻¹) with μ_0 as the vacuum permeability, $\hat{\mathbf{h}}$ is a unit vector defining the magnetization direction of all prisms with inclination m_i and declination m_d . In equation 1, ∇ is a 3D gradient operator vector given by $\nabla \equiv \left[\frac{\partial}{\partial x}, \frac{\partial}{\partial y}, \frac{\partial}{\partial z} \right]^T$ and

$$\frac{1}{r_{ij}} = \frac{1}{\sqrt{(x_i - x'_j)^2 + (y_i - y'_j)^2 + (z_i - z'_j)^2}}, \quad (2)$$

where x_i , y_i , and z_i are the coordinates of the i th observation point, x'_j and y'_j are the horizontal coordinates of the center of the j th prism, and z' is the integration variable representing the z -coordinate of an arbitrary point within the j th prism.

Equation 1 approximates the 3D integral (the volume integral) of the magnetic components of a prism by a 1D integration taken with respect to the z -axis of a prism (the prism thickness). Like Hidalgo-Gato and Barbosa (2019), we calculate the integral in equation 1 numerically using the GLQ produced by a dipole located along the vertical axis passing through the prism center. For additional details about the fast-prismatic forward modeling and the accuracy analysis of this modeling, readers can refer to Hidalgo-Gato and Barbosa (2019).

The amplitude of the magnetic anomaly vector due to the M prisms at the i th observation point (x_i, y_i, z_i) , $i = 1, \dots, N$, is given by

$$d_i(\mathbf{p}, m) = m f_i(\mathbf{p}), \quad (3a)$$

where m is the uniform magnetization intensity of the prisms and

$$f_i(\mathbf{p}) = \sqrt{\left(\sum_{j=1}^M b_{ij}^x \right)^2 + \left(\sum_{j=1}^M b_{ij}^y \right)^2 + \left(\sum_{j=1}^M b_{ij}^z \right)^2}, \quad (3b)$$

in which b_{ij}^α , $\alpha = x, y, z$, is defined by equation 1, and $\mathbf{p} = [p_1, \dots, p_M]^T$ is a vector containing the depths to the top of the M prisms.

Inverse problem

We consider the observed amplitude of the magnetic anomaly vector $\mathbf{d}^0 = [d_1^0, \dots, d_N^0]^T$ produced by a basement relief with the constant magnetization vector having intensity m , inclination m_i , and declination m_d . Let $\mathbf{d}(\mathbf{p}, m)$ be the N -dimensional vector of the predicted amplitude of the magnetic anomaly vector,

$$\mathbf{d}(\mathbf{p}, m) = m \mathbf{f}(\mathbf{p}), \quad (4)$$

whose i th element $d_i(\mathbf{p}, m)$ is given by equation 3a and $\mathbf{f}(\mathbf{p})$ is an $N \times 1$ vector whose i th element is defined by equation 3b.

Here, we wish to estimate the depths of the tops of the M prisms (\mathbf{p}) and the intensity of the magnetization vector (m) that better explain the observed amplitude \mathbf{d}^0 . Estimating the depths to the

tops of M prisms from the observed amplitude data \mathbf{d}^0 to retrieve the shape of the basement relief is a nonlinear inverse problem. Conversely, estimating the magnetization intensity is a linear inverse problem. The ill-posedness of this problem is because of the inherent ambiguity involving attempts to estimate the physical property and the volume of the source from any potential field data. To reduce this ambiguity, we impose proximity between the estimated depths and a previously defined average depth Z_{avg} .

This problem is solved by minimizing the objective function

$$\varphi(\mathbf{p}, m) = \|\mathbf{d}^0 - \mathbf{d}(\mathbf{p}, m)\|^2 + \mu\|\mathbf{p} - \mathbf{p}^a\|^2, \quad (5)$$

where $\|\bullet\|$ is the Euclidean norm, \mathbf{p}^a is an M -dimensional vector with all elements equal to Z_{avg} , and μ is a nonnegative scalar (regularizing parameter). The second Euclidean norm on the right side of equation 5 imposes a proximity between the estimated depths and the average depth Z_{avg} .

Expanding $\varphi(\mathbf{p}, m)$ in a Taylor series around the approximations \mathbf{p}^k and m^k , at the k th iteration, and keeping terms up to second order, we get

$$\begin{aligned} \varphi(\mathbf{p}^k + \Delta\mathbf{p}^k, m^k + \Delta m^k) &= \varphi(\mathbf{p}^k, m^k) + \mathbf{J}_p^{kT} \Delta\mathbf{p}^k + J_m^k \Delta m^k \\ &+ \frac{1}{2} \Delta\mathbf{p}^{kT} \mathbf{H}_{pp}^k \Delta\mathbf{p}^k + \frac{1}{2} \Delta m^k H_{mm}^k \Delta m^k + \frac{1}{2} \Delta\mathbf{p}^{kT} \mathbf{h}_{pm}^k \Delta m^k \\ &+ \frac{1}{2} \Delta m^k \mathbf{h}_{mp}^{kT} \Delta\mathbf{p}^k, \end{aligned} \quad (6)$$

where J_m^k is a scalar that contains the derivative of the function $\varphi(\mathbf{p}, m)$ with respect to m ,

$$J_m^k = -2\mathbf{d}^{0T} \mathbf{f}(\mathbf{p}^k) + 2m^k \mathbf{f}(\mathbf{p}^k)^T \mathbf{f}(\mathbf{p}^k), \quad (7)$$

and \mathbf{J}_p^k is the $M \times 1$ gradient vector of the function $\varphi(\mathbf{p}, m)$ with respect to vector \mathbf{p} ,

$$\mathbf{J}_p^k = -2[\mathbf{A}^k]^T [\mathbf{d}^0 - m^k \mathbf{f}(\mathbf{p}^k)] + 2\mu(\mathbf{p}^k - \mathbf{p}^a), \quad (8)$$

where \mathbf{A}^k is the $N \times M$ Jacobian matrix of the function $\mathbf{d}(\mathbf{p})$ with respect to vector \mathbf{p} . The ij th element a_{ij}^k of matrix \mathbf{A}^k is the derivative of $\mathbf{d}(\mathbf{p})$ (equation 3b) with respect to the depth to the top of the j th prism p_j , that is,

$$\begin{aligned} a_{ij}^k &= \frac{m^k}{f_i(\mathbf{p}^k)} \left(\sum_{j=1}^M b_{ij}^x, \sum_{j=1}^M b_{ij}^y, \sum_{j=1}^M b_{ij}^z \right) \\ &\cdot \left(\frac{\partial}{\partial p_j} b_{ij}^x, \frac{\partial}{\partial p_j} b_{ij}^y, \frac{\partial}{\partial p_j} b_{ij}^z \right), \end{aligned} \quad (9a)$$

where “.” represents the dot product and the derivative part of equation 9a is

$$\left(\frac{\partial}{\partial p_j} b_{ij}^x, \frac{\partial}{\partial p_j} b_{ij}^y, \frac{\partial}{\partial p_j} b_{ij}^z \right) = (-\phi_i^x(p_j), -\phi_i^y(p_j), -\phi_i^z(p_j)), \quad (9b)$$

where $\phi_i^\alpha(p_j)$ and $\alpha = x, y, z$, is the α -component of the magnetic induction produced by a single j th dipole at the i th observation point. The j th dipole is magnetized by induction, with unitary

magnetic moment and is located at the top of the center of the j th prism whose depth is p_j . Like [Hidalgo-Gato and Barbosa \(2019\)](#), the elements of the Jacobian matrix \mathbf{A}^k have a simple analytic expression (equations 9a and 9b) that is more computationally efficient than the numerical approximation. In equation 6, H_{mm}^k is a scalar that contains the second derivative of the function $\varphi(\mathbf{p}, m)$ with respect to m :

$$H_{mm}^k = 2\mathbf{f}(\mathbf{p}^k)^T \mathbf{f}(\mathbf{p}^k). \quad (10)$$

The term \mathbf{H}_{pp}^k is the $M \times M$ Hessian matrix of the function $\varphi(\mathbf{p}, m)$ with respect to vector \mathbf{p} :

$$\mathbf{H}_{pp}^k \approx 2\mathbf{A}^{kT} \mathbf{A}^k + 2\mu\mathbf{I}, \quad (11)$$

where \mathbf{I} is the identity matrix of order M , and \mathbf{h}_{pm}^k is an $M \times 1$ vector containing the second derivatives of the function $\varphi(\mathbf{p}, m)$ with respect to \mathbf{p} and m :

$$\mathbf{h}_{pm}^k = -2\mathbf{F}^{kT} \mathbf{d}^0 + 4m^k \mathbf{F}^{kT} \mathbf{f}(\mathbf{p}^k), \quad (12)$$

and $\mathbf{h}_{mp}^k = \mathbf{h}_{pm}^k$. In equation 12, \mathbf{F}^k is the $N \times M$ Jacobian matrix of the function $\mathbf{f}(\mathbf{p})$ with respect to vector \mathbf{p} . All functions defined by equations 7–12 are evaluated at $\mathbf{p} = \mathbf{p}^k$ and $m = m^k$.

By differentiating the expanded function $\varphi(\mathbf{p}^k + \Delta\mathbf{p}^k, m^k + \Delta m^k)$ (equation 6) with respect to $\Delta\mathbf{p}^k$ and Δm^k and setting the result equal to the null vector, we obtain the block linear systems of equations given

$$\begin{bmatrix} H_{mm}^k & \mathbf{h}_{mp}^{kT} \\ \mathbf{h}_{pm}^k & \mathbf{H}_{pp}^k \end{bmatrix} \begin{bmatrix} \Delta\hat{m}^k \\ \Delta\hat{\mathbf{p}}^k \end{bmatrix} = - \begin{bmatrix} J_m^k \\ \mathbf{J}_p^k \end{bmatrix}, \quad (13)$$

where the caret denotes estimate. Here, to estimate the magnetization intensity perturbation Δm^k and the depth-to-basement perturbation $\Delta\mathbf{p}^k$, we solve the full linear system defined by equation 13 and update the magnetization intensity and depth-to-basement estimates iteratively as follows:

$$\hat{m}^{k+1} \hat{m}^k + \Delta\hat{m}^k, \quad (14a)$$

and

$$\hat{\mathbf{p}}^{k+1} \hat{\mathbf{p}}^k + \Delta\hat{\mathbf{p}}^k. \quad (14b)$$

The stopping criterion is based on the invariance of the objective function (equation 5). At the iteration $k = 0$, the initial guest \mathbf{p}^0 of the basement depths is an M -dimensional vector with all elements equals to the average depth Z_{avg} .

We call attention to an interesting alternative approach to obtain the magnetization intensity and depth-to-basement estimates. This alternative approach is based on the fact that the vector \mathbf{h}_{pm}^k (equation 12), containing the second derivatives of $\varphi(\mathbf{p}, m)$ with respect to \mathbf{p} and m , has elements close to zero (order of 10^{-8}). Hence, the two off-diagonal blocks in the linear system of equations 13 can be neglected. This yields to a block diagonal linear system that, in turn, results in a two-step alternative approach for estimating the perturbations and $\hat{\mathbf{p}}^k$. In the first step, we solve a linear inverse problem by taking the estimate of the magnetization intensity perturbation as

$$\Delta\hat{m}^k = \hat{m}^{k+1} - \hat{m}^k, \quad (15)$$

and we estimate the magnetization intensity by

$$\hat{\mathbf{m}}^{k+1} = \frac{\mathbf{d}^0 \mathbf{f}(\mathbf{p}^k)}{\mathbf{f}(\mathbf{p}^k)^T \mathbf{f}(\mathbf{p}^k)}. \quad (16)$$

In the second step, we solve a nonlinear inversion by using the iterative Gauss-Newton method with Marquardt's (1963) strategy (Silva et al., 2001; Silva Dias et al., 2007) for estimating the depths to the basement. This is accomplished by estimating, at the k th iteration, the vector of the depth-to-basement perturbation $\Delta\hat{\mathbf{p}}^k$ through the solution of the linear equation system

$$(\mathbf{H}_{\mathbf{pp}}^k + \lambda^k \mathbf{I}) \Delta\hat{\mathbf{p}}^k = -\mathbf{J}_p^k, \quad (17)$$

where \mathbf{J}_p^k and $\mathbf{H}_{\mathbf{pp}}^k$ are given, respectively, by equations 8 and 11 and λ^k is a nonnegative number, known as Marquardt's parameter, which is automatically adjusted during the iterative process to guarantee that the modified Hessian matrix be positive definite and to ensure the convergence (Silva et al., 2001; Aster et al., 2005).

We stress that the computation time and the estimated perturbations ($\Delta\hat{\mathbf{m}}^k$ and $\Delta\hat{\mathbf{p}}^k$) obtained by solving the full linear system (equation 13) or by following the above explained alternative approach (equations 15–17) are approximately equal, in the same order of magnitude, and both satisfactorily recover the same estimated basement relief. Hence, we used the approximate alternative approach described before.

Determining the inversion hyperparameters

In an inverse problem, hyperparameters are variables whose values are set before running the inversion code. Hyperparameters affect the inversion result, but they are not directly estimated in the inversion. In our work, the hyperparameters are the regularizing parameter μ (equation 5), the average depth Z_{avg} (vector \mathbf{p}^a in equation 5), and the bottom depth Z_b (equation 1).

The regularizing parameter μ controls the solution stability and how close the estimated basement relief will be to the average depth Z_{avg} . The larger the value of μ , the more stable and closer to the average depth Z_{avg} will be the estimated basement relief. To determine μ , we use the L-curve criterion (Hansen, 1992), which consists in plotting, on a log-log scale, the squared norm of the regularized solution ($\|\hat{\mathbf{p}} - \mathbf{p}^a\|^2$) against the squared norm of the regularized data residual ($\|\mathbf{d}^0 - \mathbf{d}(\hat{\mathbf{p}}, \hat{\mathbf{m}})\|^2$) for a range of regularizing parameters. Typically, this plot resembles an L-shaped curve. The optimum value of μ is the one closest to the “corner” of the L-curve.

To determine the average depth Z_{avg} and the bottom depth Z_b , we use the spectral method originally proposed by Bhattacharyya and Leu (1977) and modified by Okubo et al. (1985). Bhattacharyya and Leu (1977) present a method for the spectral analysis of gravity and magnetic anomalies due to 3D vertical prism. This method determines the depth to the top of the source from the linear slope of the azimuthally averaged Fourier spectrum. We use this depth to the top of the source as the average basement depth Z_{avg} . Bhattacharyya and Leu (1977) also determine the depth to the centroid (Z_c) from the slope of an azimuthally averaged frequency-scaled Fourier spectrum in the low-wavenumber region. Finally, the depth to the bottom of the source Z_b is determined by the difference between $2Z_c$ and the depth to the top of the source (here called Z_{avg}), that is, $Z_b = 2Z_c - Z_{\text{avg}}$.

APPLICATION TO SYNTHETIC DATA

To demonstrate and analyze the accuracy of our method, we apply it on synthetic data simulating a rifted basin with nonmagnetic sediments overlaying the basement relief. Figure 1a (vertically exaggerated) shows the simulated basement relief parameterized with a collection of prisms equally distributed in the x - and y -directions. All of the prisms have the base at the constant surface $Z_b = 8$ km. The basement relief in Figure 1a extends from -30 to 30 km in the x - and y -directions. To minimize edge effects in the inverse problem, we extrapolate the model by 20 km outside the shown area in both horizontal directions. Figure 1b shows the noise-corrupted amplitude of the magnetic anomaly vector produced by the simulated rifted basin with a constant magnetization vector having inclination, declination, and intensity equal to $+45^\circ$, $+20^\circ$, and 2 A/m, respectively. The basement is magnetized by induction only. We use the implementation of Uieda et al. (2013) to calculate the b_x , b_y , and b_z components of the magnetic vector produced by the prisms on a regular observation grid of 0.5×0.5 (in km) at a 0.15 km height. The anomaly is corrupted with pseudorandom zero-mean Gaussian noise with standard deviation of 10 nT.

To invert the amplitude of the magnetic anomaly vector (Figure 1b), we assume an average depth Z_{avg} equal to 3.51 km. This value is equal to the true average depth of the simulated basement relief. We also assume that the basement magnetization vector (inclination and declination) is known and constant. We parameterize the simulated basement by discretizing it into 100×100 grid points of 3D vertical prisms in the x - and y -directions, respectively, with the same horizontal dimensions of 1 km. This discretization model includes the extended area beyond the horizontal limits of the data.

Because we assume the true average depth of the sediment-basement interface, the magnetization intensity is not a sensitive parameter in our inverse problem; thus, any initial constant guess of the magnetization intensity results in the same estimated basement relief for a given pair of inclination (m_i) and declination (m_d). We solved our inverse problem using $\mu = 0.01$, which was estimated through L-curve approach (Hansen, 1992). The inversion converged within 11 iterations to misfit values close to the error level.

Figure 1c shows the estimated basement relief and histograms of the differences between the simulated (Figure 1a) and estimated basement depths. The basement is recovered within less than ± 0.1 km differences (one standard deviation), and the histogram of depth residuals shows a sample mean close to zero and standard deviation of 0.078 km (Figure 1c). As we can see, the predicted data (Figure 1d) explain the observed (Figure 1b) amplitudes of the magnetic anomaly vector within the error level regardless of the wrong initial guess of the magnetization intensity (80 A/m). We recovered the magnetization intensity in the first iteration with a high accuracy level (2.02 A/m).

Sensitivity analysis to the magnetization direction

To investigate the sensitivity of our method to the magnetization direction, we invert the observed amplitude of the magnetic anomaly vector (Figure 1b) for different combinations of inclination m_i and declination m_d of the magnetization vector direction. Figures 2 and 3 display the results of this sensitivity analysis. Figure 2a shows the observed data (the same shown in Figure 1b) produced by the true simulated basement relief shown in Figure 3a (the same shown in Figure 1a) and the true basement relief profiles

(the black line) whose locations are shown in the map (the dashed lines in Figure 3a) of the true basement relief. Figures 2b and 3b show the inversion results by assuming known induced magnetization vector (i.e., $m_i = 45^\circ$ and $m_d = 20^\circ$, the same results shown in Figure 1c and 1d). Figures 2c–2g and 3c–3g show the solution's sensitivity to uncertainties in the magnetization inclination and declination. The wrongly assigned magnetic inclinations m_i and declinations m_d of Figures 2c–2g and 3c–3g are shown in their corresponding title headings.

The three rows in Figure 2c–2g show the predicted amplitudes of the magnetic anomaly vector (the upper row), the histograms of the data residuals (the middle row), and the data residuals (the lower row), where the data residuals are the differences between the ob-

served (Figure 2a) and predicted (the upper panels in Figure 2c–2g) data. The first and second rows in Figure 3c–3g show, respectively, the estimated basement reliefs and model residuals defined as the differences between true basement relief (Figure 3a) and estimated basement reliefs (the upper panels in Figure 3c–3g). For a more precise analysis, we plot the true (the black line) and the estimated (the blue line) basement reliefs in 2D profiles along the east–west and north–south directions as shown in the two lower rows of Figure 3c–3g.

Figures 2c and 3c and 2d and 3d show the inversion results by using a magnetization vector inclination equal to $+45^\circ$ (the same as the true one) and wrong declinations of -45° and $+45^\circ$, respectively. The wrong negative (Figure 3c) and the wrong positive

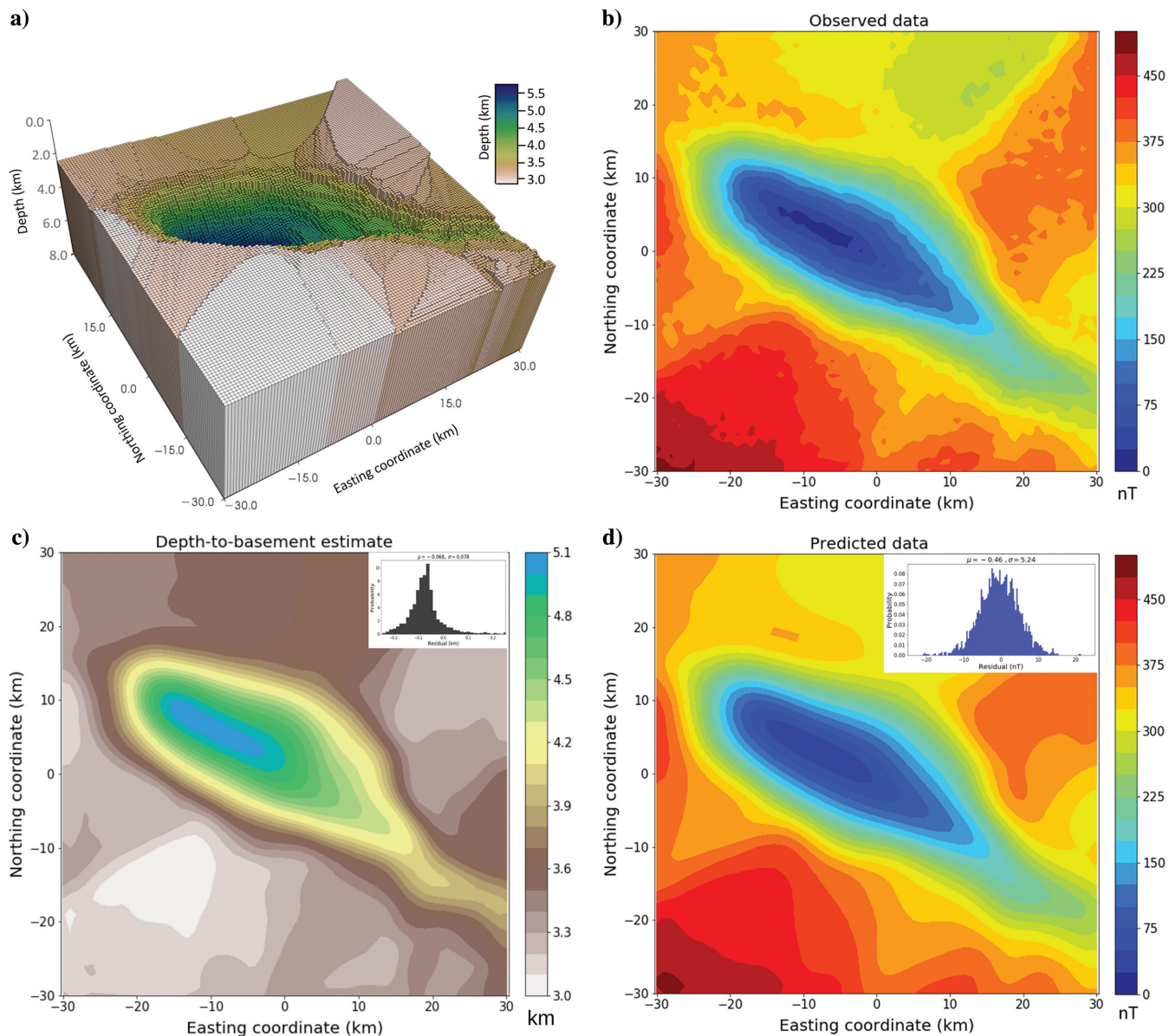


Figure 1. Synthetic data test: (a) Perspective view of the simulated basement relief with a vertical exaggeration. (b) Observed noise-corrupted amplitude of the magnetic anomaly vector. (c) Depth-to-basement estimates and the histogram of the depth residuals (the true minus the estimated basement reliefs), with its mean μ and standard deviation σ in km. (d) Predicted amplitude of the magnetic anomaly vector. The inset shows the histogram of the data residual (the observed minus the predicted data), with its mean μ and standard deviation σ in km.

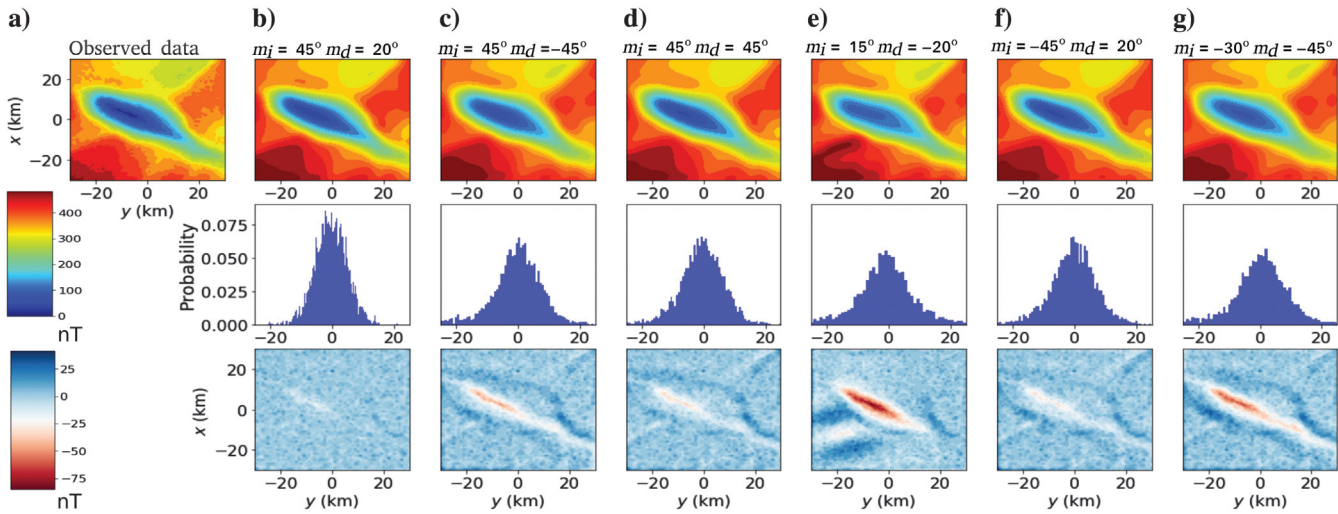


Figure 2. Magnetization direction sensibility on synthetic data. The first row shows, the observed (a) and the predicted (b–g) data for different magnetization directions (magnetic inclination m_i and declinations m_d are shown in the title headings of [b–g]). The second row shows the histogram of the data residuals (observed minus predicted) in nT and the third row is a map representation of data residuals (observed minus predicted). The true magnetization direction has inclination of $+45^\circ$ and declination of $+20^\circ$ (the estimate data shown in [b]).

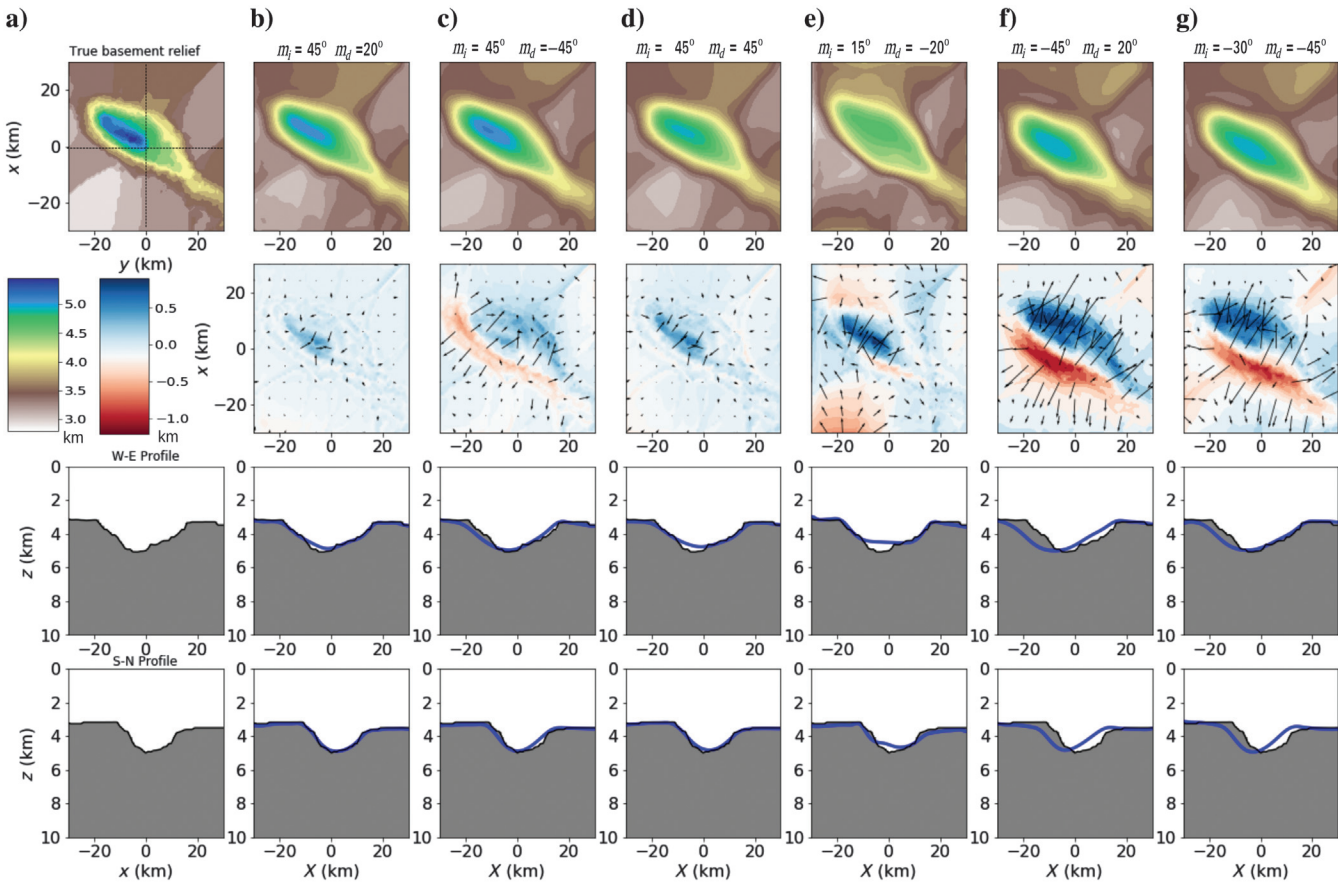


Figure 3. Magnetization direction sensibility on synthetic data. The first row shows the (a) simulated and (b–g) estimated basement relief for different magnetization directions (magnetic inclinations m_i and declinations m_d are shown in the title headings of [b–g]). The second row shows the model residuals (the true minus the estimated basement reliefs) in km. The black arrows show the gradients of the model residuals. The two lower rows show the east–west and south–north profiles extracted along the (a) true and (b–g) estimated basement reliefs. The true and estimated basement reliefs in the profiles are shown in the black and blue lines, respectively. The locations of these profiles are shown in the dashed lines in (a).

(Figure 3d) declinations satisfactorily recover the basement relief within an acceptable error margin. This is corroborated by the histograms of the data residuals in Figure 2c and 2d, which show mean and standard deviations close to zero. These results are by themselves a contribution over the existing inversion algorithms because we managed to recover the magnetic basement using a wrong declination of the magnetization vector.

The amplitude of the magnetic anomaly vector is weakly dependent on the magnetization vector direction but not fully independent, especially the opposite direction of the induced field as shown next. Figure 2e shows that even using a wrong magnetic inclination of +15° and a wrong magnetic declination of -20°, the depth-to-basement estimate (Figure 3e) recovers the simulated magnetic basement. One can notice that the estimated basement in Figure 3e is slightly different and less accurate than the estimates shown in Figure 3b–3d.

Let us now consider a negative magnetic inclination. Figure 2f shows the inversion results using magnetic inclination and declination of -45° and +20°, respectively. Note that the magnetic inclination is in the opposite direction of the true one (+45°) and the magnetic declination is equal to the true one. As we can see in Figure 2f, the predicted amplitude of the magnetic anomaly vector explains the observed data within the data error level, which is supported by the histogram of the data residuals and the data residuals. In contrast, the depth-to-basement estimate shown in Figure 3f is shifted toward the southwest direction when compared to true simulated basement relief. Similar behavior is observed in the estimated basement relief using an inclination of -30° and a declination of -45° as shown in Figures 2g and 3g. In this case, the basement relief is also shifted toward the southwest direction. However, both estimated basement reliefs shown in Figure 3f and 3g recover the shape of the true basement relief, but the estimates exhibit a small shift.

The results shown in Figures 2 and 3 suggest that the depth-to-basement estimates by inverting the amplitude of the magnetic anomaly vector are more sensitive to uncertainties in the magnetic inclination than in the magnetic declination. Figures 2c and 3c and 2d and 3d show that even considering uncertainties in magnetic declinations the amplitude data inversions retrieve the basement relief and fit the data. Conversely, Figures 2f and 3f and 2g and 3g

show that amplitude data inversions with uncertainties in the magnetic inclinations retrieve the slightly dislocated shapes of the basement reliefs. The black arrows in Figure 3 show the gradients of the model residuals defined as the differences between the true (Figure 3a) and estimated (the upper panels in Figure 3b–3g) basement reliefs. The gradients are plotted in a regular grid over the maps of the model residuals (the second row in Figure 3b–3g) where the gradients in the x- and y-directions define the direction of each arrow that points in the direction of steepest ascent and whose length is equal to the amplitude of the gradient scaled by a factor to improve the view of the arrows. Notice in Figure 3b that the arrows show the smallest lengths corroborating the excellent performance of the inversion of the amplitude data in estimating the basement relief by assuming the true magnetization vector (i.e., $m_i = 45^\circ$ and $m_d = 20^\circ$). Figure 3c and 3d shows arrow lengths smaller than the ones shown in Figure 3f and 3g certifying that the amplitude data inversions are less sensitive to uncertainties in magnetic declinations (Figure 3c and 3d). The directions of the arrows in Figure 3f and 3g indicate the displacement of the estimated basement reliefs in the southwest–northeast direction. This gradient analysis (the black arrows in Figure 3b–3g) is theoretical and cannot be applied to a field-data interpretation because it assumes knowledge of the true basement relief.

Sensitivity analysis to the average depth

In the test shown in Figure 1, the average depth Z_{avg} of the simulated basement relief was assumed to be known. To investigate the sensitivity of our method to the average depth Z_{avg} , we invert the observed amplitude of the magnetic anomaly vector (Figure 1b) by assuming a constant magnetization vector equal to the true one (inclination of +45° and declination of +20°) and a wrong average depth.

If the assigned average depth of the basement is shallower ($Z_{\text{avg}} = 1.518$ km) than the true one (3.51 km), the magnetization intensity estimate (0.5 A/m) is smaller than the true one (2 A/m) and the depth-to-basement estimate is shallower and sharper (Figure 4a) than the true one. Conversely, if the assigned average depth of the basement were deeper ($Z_{\text{avg}} = 5.518$ km) than the true one (3.51 km),

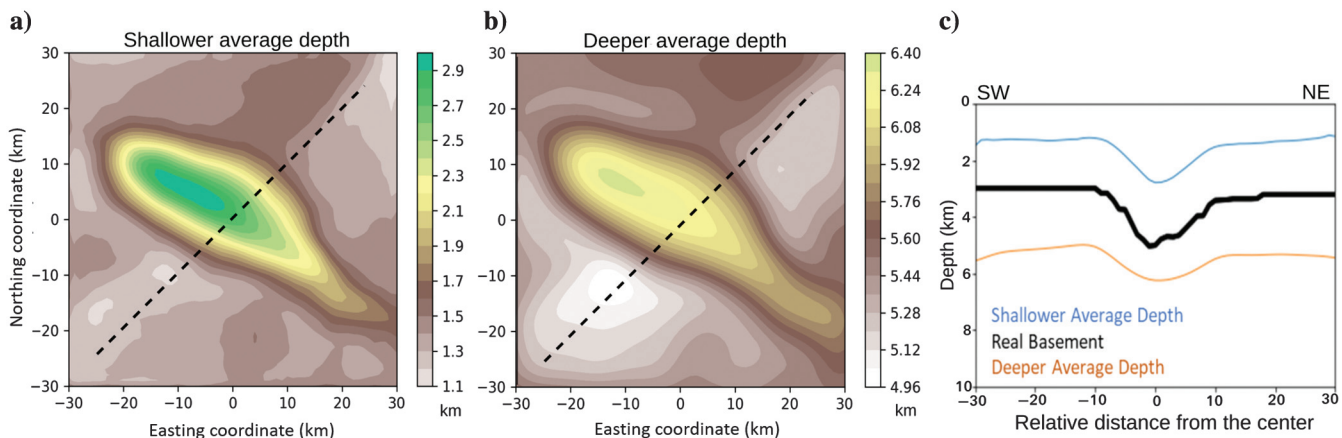


Figure 4. Average depth sensibility on synthetic data. Tests assigning incorrect average depths Z_{avg} : (a) Z_{avg} is shallower (1.518 km) than the true one, and (b) Z_{avg} is deeper (5.518 km) than the true one. (c) The southwest–northeast profiles of the true basement relief (the black line) and the estimated basements (the colored lines) shown in (a and b). The location of these profiles is shown in the dashed lines in (a and b). The true average depth of the basement relief is 3.51 km.

the magnetization intensity estimate (5 A/m) would be greater than the true one (2 A/m) and the depth-to-basement estimate (Figure 4b) would be deeper and smoother than the true one. However, in both cases (shallower or deeper average depths than the true one) the overall shapes of the estimated basement reliefs are similar (Figure 4c) but the estimated depths present different averages.

This sensitivity analysis shows that the average depth is an important hyperparameter in the inversion because of the strong coupling effects between the magnetization intensity and the basement depth. Hence, our method estimates an apparent magnetization intensity of the basement rock.

FIELD DATA APPLICATION

Geologic framework of the Foz do Amazonas Basin

The Foz do Amazonas Basin is located between French Guiana to the north and the Pará-Maranhão Basin to the southeast. Figure 5a (modified from Hidalgo-Gato and Barbosa, 2019) shows the five offshore basins that compound the Brazilian Equatorial Margin. The study area is located at the southeast portion of the Foz do Amazonas Basin (the black square), a poorly studied portion of the basin extending from shallow to deep water. We access four public wells whose locations are shown in Figure 5a called 1APS10BAP (4255 m total depth), 1APS05AP (4354 m total depth), 1AS20BAP (3542 m total depth), and 1APS37AP (2255 m total depth). Unfortunately, none of the wells drilled deep enough to penetrate the basement rocks. Notwithstanding, none of four wells drilled in the study area have shown evidence of intrasedimentary igneous intrusions. The Foz do Amazonas Basin is a magma-poor basin as described by Zalan (2017). Hence, the drillholes support the assumption of a nonmagnetic sediment layer overlaying the basement relief required by our method.

The tectonic framework of the entire Brazilian Equatorial Margin is linked to an oblique opening of the Atlantic Ocean, alternating between normal and strike-slip faults. The Precambrian basement of the Foz do Amazonas Basin consists of thrust belt faults in the north-northwest–south-southeast direction from the amalgamation

of the Gondwana. Costa et al. (2002) show a structural map with several normal faults and grabens in the onshore Foz do Amazonas and Marajó Basins. Costa et al. (2002) suggest that the onshore portions of Foz do Amazonas and Marajó Basins have steep larger border faults and multitectonic phases during the basins' evolution that includes steps such as transtension, transpression, and finalizing in another event of transtension during the Cenozoic. Indeed, there is a considerable tectonic complexity in the basement of the study area that is part of the underexplored Brazilian Equatorial Basins.

Magnetic data and basement relief estimation

The high-resolution magnetic data are from a public airborne survey over the Foz do Amazonas Basin flown between 2003 and 2004. The acquisition lines in the study area are spaced by 2 km and were flown in the N 18°W direction at a constant average height of 150 m. Figure 5a shows the acquisition polygon (blue), the study area (the black square) in geographic coordinates, and the total-field anomaly data in a local coordinate system that consists of a constant shift from the original Universal Transverse Mercator (51°W). The inclination and declination of the main geomagnetic field in the middle of the study area at the acquisition date were, respectively, 7.68° and -19.45° . We gridded the data to the constant acquisition height of 150 m.

The spectral analysis (Bhattacharyya and Leu, 1977; Okubo et al., 1985) in the total-field anomaly data (Figure 5a) shows that the average depth of the basement source (the shallow-seated source) is at 6 km depth (Figure 5b), whereas the bottom of the magnetization (the deep-seated source) is approximately 16 km depth (Figure 5c). By using the equivalent layer approach proposed by Dampney (1969), we decompose the observed total-field anomaly (Figure 5a) into the three orthogonal components of the magnetic vector b_x , b_y , and b_z and then calculate the amplitude of the magnetic vector shown in Figure 6a.

The subsurface model is discretized as a collection of prisms with tops coincident with the average basement relief ($\bar{p}^0 = 6 \text{ km}$) and the bottom at the constant surface $Z_b = 16 \text{ km}$. The prisms are regularly spaced by 3600 m in both directions with a constant magnetization vector direction equal to the main geomagnetic field and

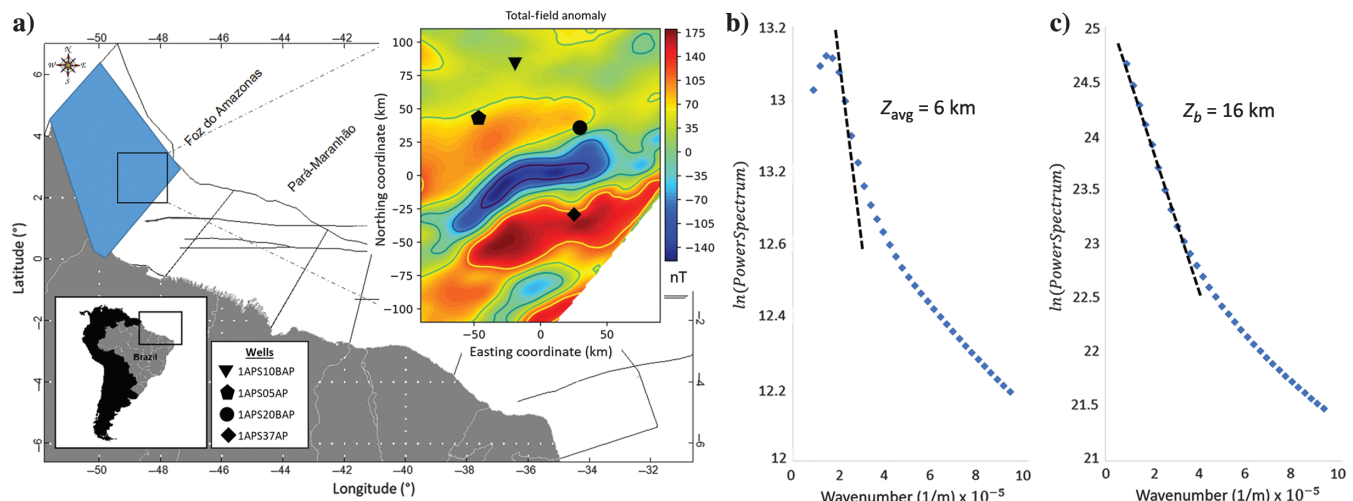


Figure 5. Real data test: (a) Location of the Foz do Amazonas Basin (Brazil) (modified from Hidalgo-Gato and Barbosa, 2019), the acquisition airborne survey (the blue polygon), the study area (the black square), and the total-field anomaly (the colored map) of the study area with well locations (the black symbols). The spectral analysis to determine (b) the average depth Z_{avg} and (c) the bottom depth Z_b .

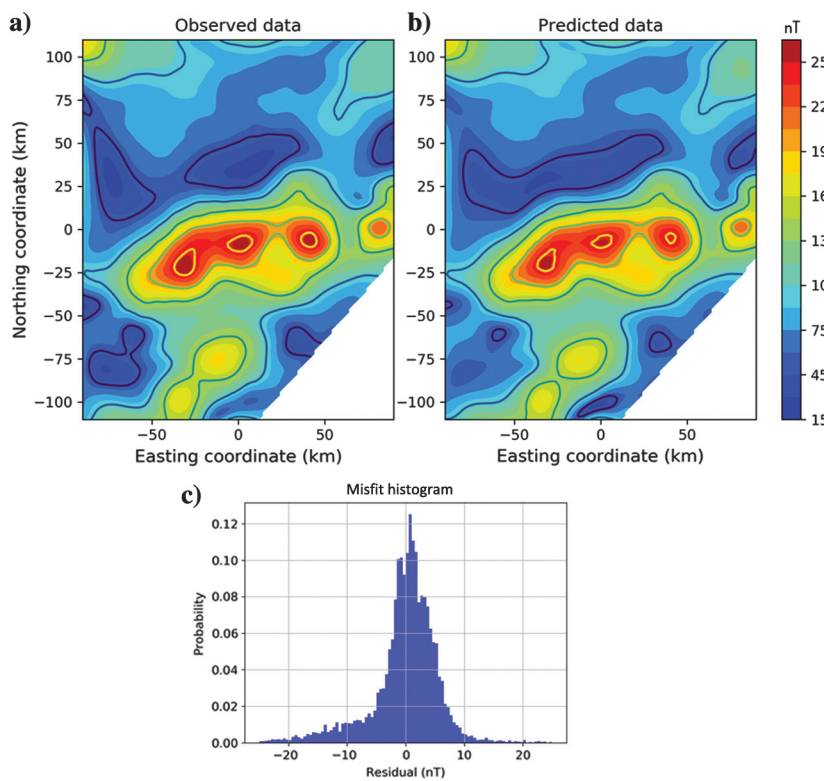


Figure 6. (a) Observed and (b) predicted amplitudes of the magnetic anomaly vector. (c) The histogram distribution of the data residual defined as the difference between (a) observed and (b) predicted data.

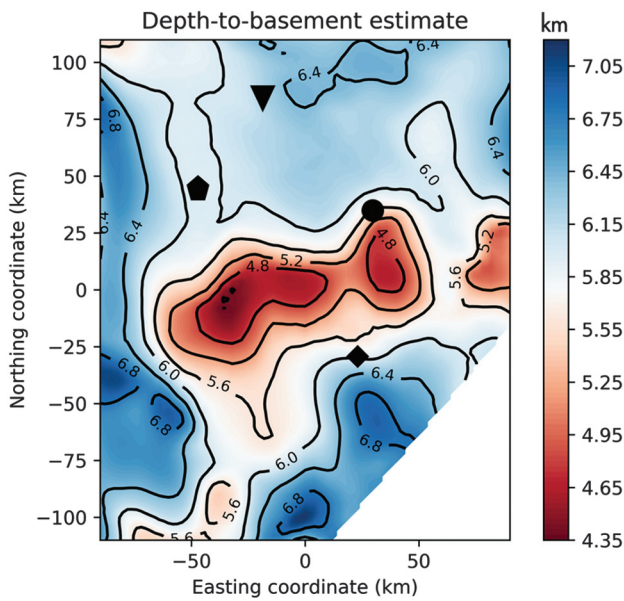


Figure 7. Contour map of the depth-to-basement estimate. The black symbols pinpoint the locations of the wells shown in Figure 5a.

intensity of 2 A/m (initial guess). We extrapolated the model by 5 km beyond the data limits in both horizontal directions to mitigate edge effects.

We inverted the amplitude of the magnetic vector (Figure 6a) to recover the basement relief using a regularization parameter $\mu = 0.001$ (estimated using the L-curve proposed by Hansen [1992]). The predicted amplitude of the magnetic vector (Figure 6b) explains the observed amplitude data (Figure 6a) within an acceptable error level. The histogram of the data residuals (Figure 6c), with 0 nT mean and standard deviation of approximately 5 nT, corroborates the acceptance of the data fitting. The recovered apparent magnetization intensity is 4 A/m. Figure 7 shows a map view of the depth-to-basement estimate with contour lines spaced by 400 m and the locations of the wells shown in Figure 5a. Two basement highs are observed in the central part of the data. Note that the transition between basement highs and lows is smooth in most of the retrieved basement. We infer that this basement feature may be due to a change in crustal domains from a continental hyperextended crust to a more homogeneous oceanic crust.

CONCLUSION

We have proposed the inversion of the amplitude of the magnetic anomaly vector to estimate the depths and the apparent magnetization intensity of the magnetized basement of a sedimentary basin. We assume that the basement rocks have a constant magnetization vector throughout the study area. Our method is weakly dependent on the magnetization vector direction and intensity; hence, the precise knowledge about them is not required. The basement relief is approximated by a collection of vertical prisms with a constant but unknown magnetization vector in direction and intensity. To overcome the ambiguity of inverting for the volume and physical property inherent to potential field data, our method requires knowledge of the average depth of the basement relief.

We calculate the predicted amplitude of the magnetic anomaly vector through a fast approach that calculates a 1D integral over the prism thickness via the GLQ. Our inverse problem uses the Gauss-Newton approximation with a proximity constraint to the average depth of the basement relief. We applied our inversion algorithm in synthetic data simulating a rifted basin and performed a sensitivity analysis by changing the magnetization direction and the average depth of the magnetized basement. We show that the amplitude of the magnetic anomaly vector is weakly dependent, but it is not completely independent of the magnetization vector direction. Our inversion results suggest that the depth-to-basement estimates are more sensitive to uncertainties in the magnetic inclination than in the magnetic declination. Because of the fundamental ambiguity consisting of the product of the physical property (the magnetization intensity) by the volume (the basement layer), uncertainties in the average depth of the basement play a significant role. If the assigned average depth of the basement is deeper than the true one, the magnetization intensity estimate is greater, and the recovered basement is deeper and smoother. However, if the assigned average depth were shallower than the true one, the magnetization intensity

estimate would be smaller and the depth-to-basement estimate would be shallower and less smooth. However, the shape of the estimated basement relief is very similar, regardless of the uncertainties in the magnetization vector direction and the average depth of the basement.

We inverted a magnetic-amplitude data set over the Foz do Amazonas Basin in the Brazilian Equatorial Margin. The amplitude data set was calculated from the observed total-field anomaly in the space domain through the equivalent layer approach. Our inversion estimates a smooth basement relief deepening to the north. In regional scale, the gradient changes in the estimated basement relief seem to characterize the transition between continental and oceanic crusts.

The main limitation of our method is the assumption about the uniform magnetization of the basement rocks. The method estimates a single apparent magnetization intensity. Hence, a future improvement to the method includes dealing with intrabasement mafic and ultramafic bodies giving rise to strongly interfering magnetic anomalies.

ACKNOWLEDGMENTS

The authors thank the editor-in-chief J. Shragge, the associate editor, and the reviewers for their constructive comments. V. C. F. Barbosa was supported by fellowships from CNPq (grant no. 307135/2014-4) and FAPERJ (grant no. E-26/202.582/2019). V. C. Oliveira Jr. was supported by fellowships from CNPq (grant no. 308945/2017-4) and FAPERJ (grant no. E-26/202.729/2018). The authors thank the Petroleum National Agency for permission to use the aeromagnetic data set.

DATA AND MATERIALS AVAILABILITY

Data associated with this research is public and can be obtained by requesting to ANP (Brazilian National Oil and Gas Agency).

REFERENCES

- Ali, M. Y., J. D. Fairhead, C. M. Green, and A. Noufal, 2017, Basement structure of the United Arab Emirates derived from an analysis of regional gravity and aeromagnetic database: *Tectonophysics*, **712**, 503–522, doi: [10.1016/j.tecto.2017.06.006](https://doi.org/10.1016/j.tecto.2017.06.006).
- Aster, R. C., B. Borchers, and C. H. Thurber, 2005, Parameter estimation and inverse problems (international geophysics): Academic Press.
- Bhattacharyya, B. K., 1964, Magnetic anomalies due to prism-shaped bodies with arbitrary polarization: *Geophysics*, **29**, 517–531, doi: [10.1190/1.1439386](https://doi.org/10.1190/1.1439386).
- Bhattacharyya, B. K., and L. K. Leu, 1977, Spectral analysis of gravity and magnetic anomalies due to rectangular prismatic bodies: *Geophysics*, **42**, 41–50, doi: [10.1190/1.1440712](https://doi.org/10.1190/1.1440712).
- Caratori Tontini, F., L. Cocchi, and C. Carmisciano, 2008, Potential-field inversion for a layer with uneven thickness: The Tyrrhenian Sea density model: *Physics of the Earth and Planetary Interiors*, **166**, 105–111, doi: [10.1016/j.pepi.2007.10.007](https://doi.org/10.1016/j.pepi.2007.10.007).
- Carvalho, J., H. Matias, T. Rabeh, P. T. L. Menezes, V. C. F. Barbosa, R. Dias, and F. Carrilho, 2012, Connecting onshore structures in the Algarve with the southern Portuguese continental margin: The Carcavai fault zone: *Tectonophysics*, 151–162, doi: [10.1016/j.tecto.2012.08.011](https://doi.org/10.1016/j.tecto.2012.08.011).
- Christensen, A. N., and M. H. Dransfield, 2002, Airborne vector magnetometry over banded iron-formations: 72nd Annual International Meeting, SEG, Expanded Abstracts, 13–16, doi: [10.1190/1.1816921](https://doi.org/10.1190/1.1816921).
- Costa, J. B. S., Y. Hasui, R. L. Bemerguy, A. V. Soares-Junior, and J. M. M. Villegas, 2002, Tectonics and paleogeography of the Marajó Basin, northern Brazil: Annals of the Brazilian Academy of Sciences, **74**, 519–531, doi: [10.1590/S0001-37652002000300013](https://doi.org/10.1590/S0001-37652002000300013).
- Dampney, C., 1969, The equivalent source technique: *Geophysics*, **34**, 39–53, doi: [10.1190/1.1439996](https://doi.org/10.1190/1.1439996).
- Dransfield, M., A. Christensen, and G. Liu, 2003, Airborne vector magnetics mapping of remanently magnetized banded iron formations at Rocklea, Western Australia: *Exploration Geophysics*, **34**, 93–96, doi: [10.1071/EG03093](https://doi.org/10.1071/EG03093).
- Gallardo-Delgado, L. A., M. A. Pérez-Flores, and E. Gómez-Treviño, 2003, A versatile algorithm for joint 3D inversion of gravity and magnetic data: *Geophysics*, **68**, 949–959, doi: [10.1190/1.1581067](https://doi.org/10.1190/1.1581067).
- Guspi, F., 1993, Noniterative nonlinear gravity inversion: *Geophysics*, **58**, 935–940, doi: [10.1190/1.1443484](https://doi.org/10.1190/1.1443484).
- Haney, M. M., C. Johnston, Y. Li, and M. N. Nabighian, 2003, Envelopes of 3D and 3D magnetic data and their relationship to the analytic signal: Preliminary results: 73rd Annual International Meeting, SEG, Expanded Abstracts, 592–595, doi: [10.1190/1.1817997](https://doi.org/10.1190/1.1817997).
- Hansen, P. C., 1992, Analysis of discrete ill-posed problems by means of the L-curve: *SIAM Review*, **34**, 561–580, doi: [10.1137/1034115](https://doi.org/10.1137/1034115).
- Hidalgo-Gato, M. C., and V. C. F. Barbosa, 2015, Edge detection of potential-field sources using scale-space monogenic signal: Fundamental principles: *Geophysics*, **80**, no. 5, J27–J36, doi: [10.1190/geo2015-0025.1](https://doi.org/10.1190/geo2015-0025.1).
- Hidalgo-Gato, M. C., and V. C. F. Barbosa, 2019, Fast 3D magnetic inversion of a surface relief in the space domain: *Geophysics*, **84**, no. 5, J57–J67, doi: [10.1190/geo2018-0712.1](https://doi.org/10.1190/geo2018-0712.1).
- Li, Y., S. E. Shearer, M. M. Haney, and N. Dannemiller, 2010, Comprehensive approaches to 3D inversion of magnetic data affected by remanent magnetization: *Geophysics*, **75**, no. 1, L1–L11, doi: [10.1190/1.3294766](https://doi.org/10.1190/1.3294766).
- Lourenco, J., P. T. L. Menezes, and V. C. F. Barbosa, 2014, Connecting onshore-offshore Campos Basin structures: Interpretation of high-resolution airborne magnetic data: *Interpretation*, **2**, no. 4, SJ181–SJ191.
- Lourenco, J. S., and H. F. Morrison, 1973, Vector magnetic anomalies derived from measurements of a single component of the field: *Geophysics*, **38**, 359–368, doi: [10.1190/1.1440346](https://doi.org/10.1190/1.1440346).
- Marquardt, D. W., 1963, An algorithm for least-squares estimation of nonlinear parameters: *Journal of the Society for Industrial and Applied Mathematics*, **11**, 431–441, doi: [10.1137/0111030](https://doi.org/10.1137/0111030).
- Mickus, K. L., and W. J. Peeples, 1992, Inversion of gravity and magnetic data for the lower surface of a 2.5 dimensional sedimentary basin: *Geophysical Prospecting*, **40**, 171–193, doi: [10.1111/j.1365-2478.1992.tb00370.x](https://doi.org/10.1111/j.1365-2478.1992.tb00370.x).
- Nabighian, M. N., 1972, The analytic signal of two-dimensional magnetic bodies with polygonal cross-section: Its properties and use for automated anomaly interpretation: *Geophysics*, **37**, 507–517, doi: [10.1190/1.1440276](https://doi.org/10.1190/1.1440276).
- Nabighian, M. N., 1984, Toward a three-dimensional automatic interpretation of potential field data via generalized Hilbert transforms: Fundamental relations: *Geophysics*, **49**, 780–786, doi: [10.1190/1.1441706](https://doi.org/10.1190/1.1441706).
- Nunes, T. M., V. C. F. Barbosa, and J. B. C. Silva, 2008, Magnetic basement depth inversion in the space domain: *Pure and Applied Geophysics*, **165**, 1891–1911, doi: [10.1007/s00024-008-0405-x](https://doi.org/10.1007/s00024-008-0405-x).
- Okubo, Y., R. J. Graf, R. O. Hansen, K. Ogawa, and H. Tsu, 1985, Curie point depths of the island of Kyushu and surrounding areas, Japan: *Geophysics*, **50**, 481–494, doi: [10.1190/1.1441926](https://doi.org/10.1190/1.1441926).
- Oldenburg, D. W., 1974, The inversion and interpretation of gravity anomalies: *Geophysics*, **39**, 526–536, doi: [10.1190/1.1440444](https://doi.org/10.1190/1.1440444).
- Parker, R. L., 1973, The rapid calculation of potential anomalies: *Geophysical Journal of the Royal Astronomical Society*, **31**, 447–455, doi: [10.1111/j.1365-246X.1973.tb06513.x](https://doi.org/10.1111/j.1365-246X.1973.tb06513.x).
- Pedersen, L. B., 1978, Wavenumber domain expressions for potential fields from arbitrary 2-, 2-1/2-, and 3-dimensional bodies: *Geophysics*, **43**, 626–630, doi: [10.1190/1.1440841](https://doi.org/10.1190/1.1440841).
- Shearer, S., and Y. Li, 2004, 3D inversion of magnetic total gradient data in the presence of remanent magnetization: 74th Annual International Meeting, SEG, Expanded Abstracts, 774–777, doi: [10.1190/1.1851318](https://doi.org/10.1190/1.1851318).
- Silva, J. B. C., W. E. Medeiros, and V. C. F. Barbosa, 2001, Pitfalls in nonlinear inverse problem: *Pure and Applied Geophysics*, **158**, 945–964, doi: [10.1007/PL00001215](https://doi.org/10.1007/PL00001215).
- Silva Dias, F. J. S., V. C. F. Barbosa, and J. B. C. Silva, 2007, 2D gravity inversion of a complex interface in the presence of interfering sources: *Geophysics*, **72**, no. 2, I13–I22, doi: [10.1190/1.2424545](https://doi.org/10.1190/1.2424545).
- Spector, A., and F. S. Grant, 1970, Statistical models for interpreting aeromagnetic data: *Geophysics*, **35**, 293–302, doi: [10.1190/1.1440092](https://doi.org/10.1190/1.1440092).
- Uieda, L., V. C. Oliveira, Jr., and V. C. F. Barbosa, 2013, Modeling the Earth with Fatiando a Terra: Techniques: 12th Python in Science Conference, SCIPY, 90–96.
- Zalan, P. V., 2017, The differential petroleum potential of the spectrum of types of passive margins: SBGF, 15th International Congress of the Brazilian Geophysical Society.
- Zeyen, H., and J. Pous, 1991, A new 3-D inversion algorithm for magnetic total field anomalies: *Geophysical Journal International*, **104**, 583–591, doi: [10.1111/j.1365-246X.1991.tb05703.x](https://doi.org/10.1111/j.1365-246X.1991.tb05703.x).



Marlon C. Hidalgo-Gato received a B.S. (2011) in geophysics at USP, University of São Paulo, Brazil, and an M.S. (2015) and Ph.D. (2019) in geophysics at ON, National Observatory, Brazil. From 2011 to 2013, he worked as a geophysicist at FUGRO with data acquisition, processing, and interpretation. From 2013 to 2018, he worked as an R&D geophysicist

and with seismic processing at CGG. Currently, he is working as an exploration geophysicist at Shell, Brazil. His current research interests include inverse problems, optimization, and interpretation of potential-field data. He is a member of SEG and EAGE.



Valéria C. F. Barbosa received a B.S. (1986) in geology from the Federal Rural University of Rio de Janeiro, Brazil, and an M.S. (1991) and Ph.D. (1998) in geophysics from the Federal University of Pará. From 1987 to 1989, she worked as a geologist at Geopetro Consult. Geofísica Ltda. From 1998 to 2006, she worked as a scientific researcher at

LNCC, National Laboratory for Scientific Computing, Brazil. From 2014 to 2016, she was the coordinator of the Geophysics and Astronomy Graduate Study Programs. From 2005 to 2017 and from 2017 to 2018, she served as associate and assistant editors of *GEOPHYSICS*, respectively. From 2013 to 2017, she served as the editor of *Pure and Applied Geophysics*. Currently, she is working as a research geophysicist at ON, National Observatory, Brazil. Her current research interests include inverse problems, optimization, and interpretation of potential-field data. She is a member of SEG, EAGE, and AGU.



Vanderlei C. Oliveira Jr. received a B.S. (2008) in geophysics from the University of São Paulo, Brazil, and an M.S. (2010) and Ph.D. (2013) in geophysics from the National Observatory, Brazil. Currently, he is a researcher at the Department of Geophysics of the National Observatory, Brazil. His current research interests include inverse problems and potential field methods. He is a member of SEG and EAGE.